An Adaptive Actuator Driver for AC Contactors

Changkun Zhang and Zhihong Xu, *Member, IEEE*

***Abstract*—The actuator drivers are rarely transplanted among different contactors because the self-tuning of excitation control parameters either takes a long time or is relevant to many contactor structural parameters. An adaptive actuator driver for ac contactors is proposed based on the coil impedance estimation and mathematical equations between the coil impedance and excitation control parameters. The coil impedance estimation and its error correction are established through the voltage balance equation when the contactor is in the open position. The coil inductance estimation is established through the zero-state response equation when the contactor is in the closed position. The mathematical equations are established based on the equivalence of the electromagnetic force under different excitation methods, the power consumption model, and the control system's transfer function. A geometric feature of the flux linkage waveform is established to identify whether a contactor is in the closed position and realize the self-transition of the driver's working state. Then, self-tuning regulators for the excitation control parameters are realized. This driver has a plug-and-play function for ac contactors and can reduce the contactor's power consumption. This driver may be prospectively reduced to a chip.**

***Index Terms*—Actuator, contactor, estimation, self-tuning regulator.**

I. Introduction

CONTACTORS, as a basic electrical apparatus, are widely used in many applications, such as motor systems [1] and power systems [2]. With the development of the smart grid and energy-saving approaches, the demand for excellent contactor performance is gradually increasing, especially for low power consumption. The operation of contactors involving high power consumption impacts the power quality of the control power supply and reduces the power efficiency of the industrial system [3], [4]. In the miniaturization trend of low-voltage ac contactors, the main method to improve the contactor performance is to establish an actuator driver based on a power electronic circuit and an automatic control scheme. The driver can adjust the excitation energy in real time to reduce the power consumption of the contactor. However, the excitation control parameters are closely related to the structure parameters of the contactor, which makes it difficult for the actuator driver to be transplanted among different contactors without any adjustment [5], [6], [7]. Low-voltage ac contactors have many specifications, so considerable resources must be spent to match the control parameters to the contactors one by one. Therefore, it is necessary to establish an actuator driver that can adapt to changes in ac contactor specifications.

The main ideas of existing contactor adaptive control schemes are as follows.

In the excitation current closed-loop control scheme, the self-tuning of the excitation current reference is based on long-duration parameter scanning and the determination of whether the contactor is in the closed position [8]. This determination is based on the current variation phenomena caused by the electromotive force [9], [10]. The electromotive force is related to the contactor structural parameters. Hence, there are some conditions in which the excitation voltage can overcome the electromotive force to stabilize the current, leading to the failure of current reference self-tuning.

Based on the common phenomenon that an air gap change leads to a flux linkage change under a constant excitation current, the flux linkage closed-loop control scheme is used to automatically adjust the current [11]. The flux linkage reference is self-tuned by parameter scanning [12]. However, the flux linkage should be acquired by an integrated observer during the excitation current adjustment process, and the observer must be sufficiently precise to avoid control failure.

According to the contact electrical signal acquired by physical sensors and the iteration algorithm, the excitation control parameters can be self-tuned after several operations of the contactor [13], [14]. Although this scheme has a good universality for different contactors, the contactors need to be equipped with physical sensors. These sensors may make the contactor lose its physical fracture, negatively impact the dielectric properties of the contactor, or be affected by the load type and arc. In addition, the initial value and iteration of excitation control parameters directly affect the performance and reliability of the contactor. As a result, when this scheme is carried out, the contactor needs to be separated from its application system or the application system must have sufficient compatibility with the change in the contactor's performance.

Manuscript received 22 December 2022; revised 28 March 2023; accepted 27 April 2023. Date of publication 15 May 2023; date of current version 27 October 2023. This work was supported in part by the National Natural Science Foundation of China under Grant 52277136, and in part by the Fujian Provincial Department of Science and Technology under Grant 2021Y4002. *(Corresponding author: Zhihong Xu.)*

Changkun Zhang is with the School of Marine Engineering, Jimei University, Xiamen 361021, China, and also with the College of Electrical Engineering and Automation, Fuzhou University, Fuzhou 350108, China (e-mail: 202372000104@jmu.edu.cn).

Zhihong Xu is with the College of Electrical Engineering and Automation, Fuzhou University, Fuzhou 350108, China, and also with the Fujian Key Laboratory of New Energy Generation and Power Conversion, Fujian Engineering Research Center of Smart Distribution Grid Equipment, Fuzhou 350108, China (e-mail: fdxzh@fzu.edu.cn).

Color versions of one or more figures in this article are available at https://doi.org/10.1109/TIE.2023.3274852.

Digital Object Identifier 10.1109/TIE.2023.3274852

Instead of physical sensors, a sensorless adaptive control scheme can be established through mathematical observers that observe the displacement or velocity of the armature [15], [16]. These observers are based on the actuator model and can be used to set the excitation parameters quickly. However, mathematical observers contain many contactor structural parameters, and changes in structural parameters will affect the accuracy of observers and the control performance [17], [18]. In addition, the reference of displacement or velocity is set based on the present nonlinear relationship between the mechanical quantities and the performance of the contactor [19]. When this scheme is applied on different contactors, the actuator model needs to be re-established, and the observers need to be calibrated.

The above adaptive schemes make it difficult to realize actuator driver transplantation seamlessly among different contactors with different specifications because of the long duration of excitation control parameter self-tuning, strong correlation of the contactor structural parameters, error sensitivity of contactor working process observation, or the need for physical sensors.

For the driver, the actuator of the contactor can be considered an ohmic-inductive load whose inductance can change, and the variation in the contactor structural parameters can be reflected in the impedance. From the perspective of the driver, we establish mathematical equations between the coil impedance and excitation control parameters and a criterion for whether the contactor is in the closed position based on a geometric feature of the flux linkage waveform. Thus, the excitation control parameters can be self-tuned based on the estimated coil impedance, and the driver has a plug-and-play function when it transplants among contactors with different specifications. In our previous work, some of the mathematical equations were established experimentally [20], and the criterion was established based on the high-pass filtered flux linkage and a threshold [11]. However, it is still necessary to mathematically explain the relationship between the coil impedance and control parameters, eliminate the threshold in the criterion, and establish self-tuning regulators of control parameters when the contactor is in the closed position.

The main contributions of this study are as follows.

1) The mathematical equations between the excitation control parameters and the coil impendence simplify the actuator model, shortening the duration of excitation control parameter self-tuning and reducing the number of contactor structural parameters involved in contactor adaptive control.
2) A geometric feature of the flux linkage waveform is established to identify whether the contactor is in the closed position through the monotonicity reversion of the geometric feature. No threshold is required for this method. This method has good compatibility with the flux linkage observation error and improves the universality of adaptive control.
3) The proposed adaptive actuator driver does not need to install physical sensors on the contact or the armature and does not need to establish the actuator model. Compared with the existing scheme, it is more suitable to realize energy-saving operations of the traditional ac contactors that are in service. The adaptive actuator driver is verified by four contactors with different specifications in experiments.

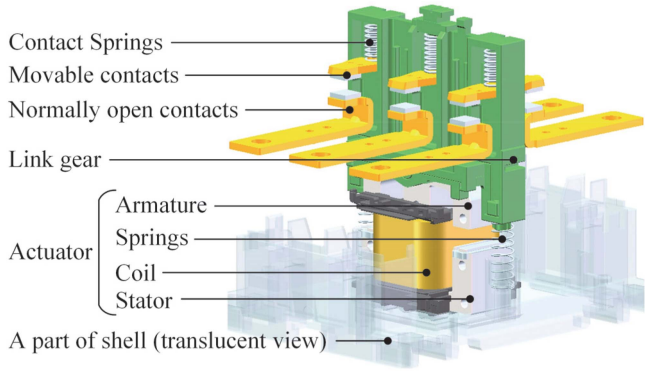

Fig. 1. Main structure of the AC contactor.

The rest of this article is organized as follows. Section II describes the structure and working principle of the ac contactor and adaptive actuator driver. Section III presents the coil impedance estimation method. In Sections IV and V, the mathematical equations between the coil impedance and control parameters for different working states of the driver are established. Section VI shows the experimental results. Finally, Section VII concludes the article.

II. Principle

The main structure of the ac contactor is shown in Fig. 1. The actuator includes an armature, a stator, a coil, and springs. When the armature and stator are separate and relatively stationary, the contactor is in the open position. When they are closed and relatively stationary, the contactor is in the closed position. By adjusting the excitation energy of the armature, the driver can change the relationship between the electromagnetic force and the resistant force and operate the contactor. The operation for bringing the armature from the open position to the closed position and keeping it in the closed position is the closing operation. In the closing operation, the driver is first in the high-power output state (HPO state). The driver outputs a high power to make the armature move. Then, when the contactor is in the closed position, the driver reduces the output power and enters the low-power output state (LPO state) to reduce the power consumption and keep the contactor in the closed position. The operation for bringing the contactor from the closed position to the open position is the opening operation. In this process, the driver reduces the electromagnetic force and makes the armature and stator separate.

The working principle of the adaptive actuator driver is shown in Fig. 2. The excitation control circuit is based on a buck circuit. VT_1 and VT_2 are metal-oxide-semiconductor field-effect transistors controlled by pulse width modulation (PWM) signals with duties d_1 and d_2, respectively. VD is a diode. ZD is a transient suppression diode. u is the bus voltage. i is the coil current. The actuator is equivalent to an ohmic-inductive load.

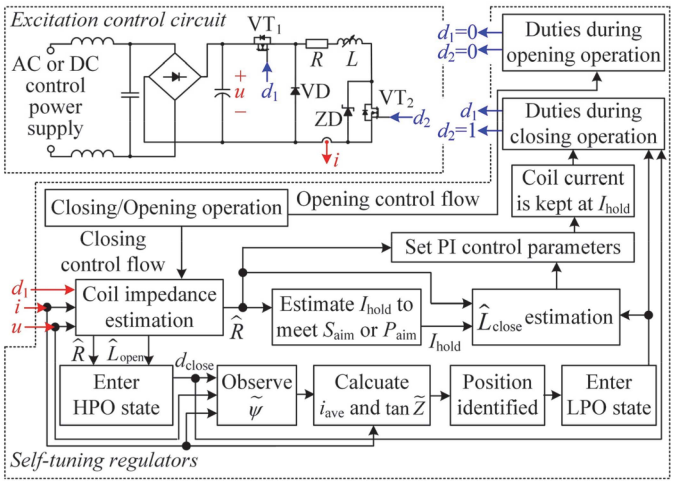

Fig. 2. Working principle of the proposed adaptive actuator driver.

R is the coil resistance, and L is the coil inductance. L is a lumped parameter that includes the magnetic diffusion in the actuator and changes because of the motion of the armature or the nonlinearity of magnetic materials. We note that L is L_{open} or L_{close} when the contactor is in the open position or the closed position, respectively.

The working process of the driver is divided into closing and opening control flows as follows.

The closing control begins once the closing operation signal is identified. First, the contactor is excited with a small d_1 and a full d_2. The contactor is kept in the open position. u, d_1, and i are collected to estimate the coil impedance. $\hat{R}$ is the estimated R, and $\hat{L}_{\text{open}}$is the estimated L_{open}. Second, the driver configures the PWM duty d_{close} based on $\hat{R}$ and $\hat{L}_{\text{open}}$ and makes d_1 d_{close}. Then, the driver enters the HPO state. At the same time, the coil current reference I_{hold} for the LPO state of the driver is set based on $\hat{R}$ and the aimed apparent or active power consumption (S_{aim} or P_{aim}). Meanwhile, the observed flux linkage $\tilde{\psi}$, the observed geometric feature of flux linkage waveform $\tan\tilde{Z}$, and the average coil current i_{ave} are used to identify whether the contactor is in the closed position. When the contactor is in the closed position, the driver enters the LPO state, and i begins to decrease. When i approaches I_{hold}, $\hat{L}_{\text{close}}$, which is the estimated L_{close}, is obtained, and the proportion-integral (PI) control parameters are set. Finally, i is stabilized at I_{hold}, and the power consumption is near the aim.

The opening control begins once the opening operation signal is identified. During the opening control, d_1 and d_2 remain at zero. ZD generates a negative voltage at the coil, and the negative voltage amplitude is the breakdown voltage of ZD. The coil current rapidly drops to zero and remains at zero. The breakdown voltage of ZD is as large as possible to fully release the mechanical breaking performance of the contactor [21]. In addition, the breakdown voltage of ZD only affects the drain-to-source breakdown voltage of VT_2 in the excitation control circuit.

III. Coil Impedance Estimation and Error Correction

A. Coil Impedance in the Open Position

The coil impedance estimation method is established according to the voltage balance equation. The coil voltage is equivalent to the product of u and d_1 to miniaturize the driver. Therefore, the coil impedance estimation will be affected by the voltage drop of the semiconductor component.

We assume that the coil impedance estimation error is only related to the drain-source on-state resistance R_{on} of VT_1 and the forward voltage drop u_{F} of VD. According to the circuit averaging method [22]

$$L_{\text{open}}\Delta i/T = (u - iR_{\text{on}})\ d_1 - iR - u_{\text{F}}\,(1 - d_1) \tag{1}$$

where T is the data update period and Δi is the change in the averaged coil current in adjacent data update cycles. Let d_1 be a constant d, keep the actuator in the open position, and take the kth and jth data points to construct a linear equation. By ignoring R_{on} and u_{F}, the estimated coil impedance is

$$\begin{cases} \hat{R} = \left(u_{(k)}\Delta i_{(j)} - u_{(j)}\Delta i_{(k)}\right) d/\left(i_{(k)}\Delta i_{(j)} - i_{(j)}\Delta i_{(k)}\right) \\ \hat{L}_{\text{open}} = \left(u_{(k)}i_{(j)} - u_{(j)}i_{(i)}\right) dT/\left(i_{(k)}\Delta i_{(j)} - i_{(j)}\Delta i_{(k)}\right) \end{cases}. \tag{2}$$

The estimation error is

$$\begin{cases} e_R = \frac{\left(i_{(j)}\Delta i_{(k)} - i_{(k)}\Delta i_{(j)}\right)dR_{\text{on}}}{i_{(k)}\Delta i_{(j)} - i_{(j)}\Delta i_{(k)}} \\ \qquad\quad - \frac{\left(\Delta i_{(k)} - \Delta i_{(j)}\right)(1-d)u_{\text{F}}}{i_{(k)}\Delta i_{(j)} - i_{(j)}\Delta i_{(k)}} \\ e_L = \frac{\left(\Delta i_{(k)} - \Delta i_{(j)}\right)(1-d)u_{\text{F}}T}{i_{(k)}\Delta i_{(j)} - i_{(j)}\Delta i_{(k)}} \end{cases}. \tag{3}$$

We note that

$$r = \frac{\Delta i_{(j)} - \Delta i_{(k)}}{i_{(k)}\Delta i_{(j)} - i_{(j)}\Delta i_{(k)}}, l = \frac{\left(i_{(j)} - i_{(k)}\right)T}{i_{(k)}\Delta i_{(j)} - i_{(j)}\Delta i_{(k)}}. \tag{4}$$

Therefore, the estimation error model is established as

$$\hat{R} = \sigma + \gamma_1 r,\ \hat{L}_{open} = \beta + \gamma_2 l \tag{5}$$

where σ is equivalent to $R + dR_{\text{on}}$, β is equivalent to L_{open}, and γ_1 and γ_2 are equivalent to $(1-d)u_{\text{F}}$ in $\hat{R}$ and $\hat{L}_{\text{open}}$, respectively. For $\hat{R}$, e_{R} is divided between σ and γ_1. For $\hat{L}_{\text{open}}$, e_{L} is located at γ_2. Therefore, the mutual influence of e_{R} and e_{L} is avoided, and the decoupling of e_{R} and e_{L} and the independent error correction of $\hat{R}$ and $\hat{L}_{\text{open}}$ are achieved. σ and β are acquired from $\hat{R}$, $\hat{L}_{\text{open}}$, r, and l with the least squares method. σ is regarded as the corrected estimation $\hat{R}'$ of the coil resistance based on the small dR_{on}. β is the corrected estimation $\hat{L}'_{\text{open}}$ of the coil inductance.

B. Coil Impedance in the Closed Position

When the contactor is in the closed position and the driver changes from the HPO state to the LPO state, VT_1 is OFF, VT_2 is ON, and the coil current decreases gradually. The estimation of L_{close} is performed when the coil current is close to I_{hold} to suppress the inductance changes caused by the nonlinearity of magnetic materials. We assume that L_{close} is constant. Then, the coil current satisfies

$$i = -u_{\text{F}}/R + (I_0 + u_{\text{F}}/R)\exp\left(-Rt/L_{\text{close}}\right) \tag{6}$$

where I_0 is the initial current. If the coil current drop Δi_{down} takes Δt, according to the first-order Taylor expansion of (6) and the ignition of u_{F}, the estimation of L_{close} is

$$\hat{L}_{\text{close}} \approx iR\Delta t/\Delta i_{\text{down}}. \tag{7}$$

The relative error of $\hat{L}_{\text{close}}$ is

$$\delta_{\text{L}} = \left|1 + i\ln\left[1 - R\Delta i_{\text{down}}/\left(Ri + u_{\text{F}}\right)\right]\right|. \tag{8}$$

$\hat{L}_{\text{close}}$ is used to set the PI control parameters for the LPO state of the driver. The PI control parameters are compatible with the estimation error of coil inductance. Therefore, although δ_{L} gradually increases with increasing Δi_{down}, Δi_{down} should still be as large as possible on the premise of a small δ_{L} to reduce the influence of sampling noise.

IV. Self-Tuning Regulator for the HPO State

A. PWM Duty

During the quasistatic motion of the armature, the closing operation of the contactor is reliable when the process satisfies

$$\forall x_{\text{arma}} \in [0, \delta), \int_0^t \left[\left(F_{\text{mag}} - f\right)/m\right] \mathrm{d}t > 0 \tag{9}$$

where x_{arma} is the displacement of the armature, δ is the stroke of the armature, F_{mag} is the electromagnetic force, f is the resistant force, and m is the mass of moving parts.

By ignoring the core reluctance and leakage flux, F_{mag} is

$$F_{\text{mag}} = \mu_0 A(Ni)^2 / \left[2(\delta - x_{\text{arma}})^2\right] \tag{10}$$

where μ_0 is the vacuum permeability, A is the total area of magnetic poles, and N is the number of coil turns. According to (10), (9) can be written as

$$\forall x_{\text{arma}} \in [0, \delta), \frac{\mu_0 A(Ni)^2}{2(\delta - x_{\text{core}})^2} \int_0^t i^2 \mathrm{d}t > \int_0^t f \mathrm{d}t. \tag{11}$$

When an ac control power supply is directly applied to the coil, i.e., ac excitation, and the air gap between the armature and stator is fixed, the coil current is

$$\begin{aligned} i = {} & \sqrt{2}U_S \cos(\theta + \xi) \exp(-Rt/L) / \sqrt{R^2 + (\omega L)^2} \\ & + \sqrt{2}U_S \cos(\omega t + \theta + \xi) / \sqrt{R^2 + (\omega L)^2} \end{aligned} \tag{12}$$

where U_{S} is the root mean square (RMS) of the ac control supply voltage, ω is the angular frequency of the ac control supply voltage, θ is the initial excitation phase, and $\sin\xi = R/\sqrt{R^2 + (\omega L)^2}$. When the motion of the armature is reliable under ac excitation, it can be seen from (11) and (12) that the motion of the armature is reliable when the RMS of the steady-state component of the coil current I_{rms} under an excitation control scheme is not less than that under ac excitation in any air gap.

In summary, the control parameters should guarantee

$$\forall x_{\text{arma}} \in [0, \delta), I_{\text{rms}} > U_{\text{S}}/\sqrt{R^2 + (\omega L)^2}. \tag{13}$$

Due to the miniaturization of the driver, the capacitance of the rectifier filter capacitor in the excitation control circuit cannot take a large value. When the driver is in the HPO state, the coil current is large, and u is a pulsating dc voltage under the ac control power supply. According to the Fourier decomposition of u, when the air gap and PWM duty d_{close} are fixed, the coil current is

$$\begin{aligned} i = {} & -2\sqrt{2}U_S d_{\text{close}} \exp(-Rt/L) / \left[9\pi R\left(4\omega^2 L^2 + R^2\right)\right] \\ & \times \left(36\omega^2 L^2 + 4\omega LR\sin\theta + 2R^2\cos\theta + 9R^2\right) \\ & + \left[4\omega LR\sin(2\omega t + \theta) + 2R^2\cos(2\omega t + \theta)\right. \\ & \left. + 36\omega^2 L^2 + 9R^2\right] 2\sqrt{2}U_S d_{\text{close}} / \left[9\pi R\left(4\omega^2 L^2 + R^2\right)\right]. \end{aligned} \tag{14}$$

The RMS of the steady-state component of the coil current described in (14) is

$$I_{\text{rms}} = 2\sqrt{2}U_{\text{S}} d_{\text{close}} \sqrt{324\omega^2 L^2 + 83R^2} / \left(9\pi R\sqrt{4\omega^2 L^2 + R^2}\right). \tag{15}$$

If I_{rms} is the same as the RMS of the current steady-state component under ac excitation, d_{close} should be self-tuned according to the change in L because L gradually increases during the motion of the armature. However, L is hard to acquire because of the flux linkage observation error. Hence, d_{close} is set according to L_{open}, which is the smallest value of L and is held constant throughout the motion of the armature.

When the contactor is excited directly by an ac source, there is a minimum control supply voltage $U_{\text{close(min)}}$. According to the contactor standard (GB14048.4), $U_{\text{close(min)}}$ should not exceed 85% of the minimum rated control supply voltage $U_{\text{e(min)}}$. The ratio of $U_{\text{close(min)}}$ to $U_{\text{e(min)}}$ is usually lower than 85% in applications. Therefore, with an ac control power supply, the mathematical equation of PWM duty for the HPO state is

$$\begin{aligned} d_{\text{close}} = {} & \left[9\pi R\kappa U_{\text{e(min)}} / \left(2\sqrt{2}U_{\text{S}}\right)\right] \sqrt{4\omega^2 L_{\text{open}}^2 + R^2} / \\ & \sqrt{\left(324\omega^2 L_{\text{open}}^2 + 83R^2\right)\left(\omega^2 L_{\text{open}}^2 + R^2\right)} \end{aligned} \tag{16}$$

where κ is the ratio of $U_{\text{close(min)}}$ to $U_{\text{e(min)}}$. In addition, the mathematical equation with a dc control power supply can be obtained analogically.

B. Transition Between the HPO State and LPO State

After the armature and the stator are closed, the driver should enter the LPO state automatically and make the contactor hold at the closed position with low power consumption.

When the control power supply is dc, or when the control power supply is ac and the rectifier filter capacitance is large, u is constant, and the coil current and flux linkage ψ are stable during the motion of the armature. The high-pass filtered flux linkage and a threshold can be used to determine whether the contactor is reliably closed, and the self-transition of the driver between the HPO state and the LPO state is realized [11]. However, u, i, and ψ fluctuate greatly when the capacitance of the rectifier filter capacitor is small and the control power supply is ac. The change in high-pass filtered flux linkage from the changes in air gap is hardly distinguished by a threshold because of the fluctuation of ψ, which limits the adaptability of this method.

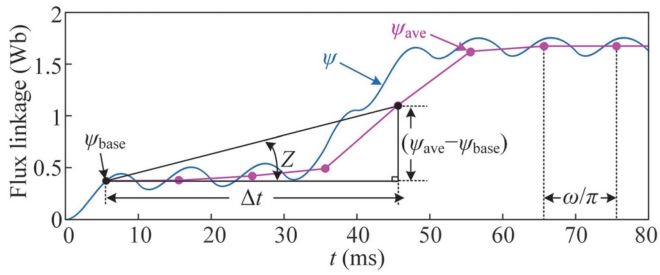

Fig. 3. Geometric feature of the flux linkage waveform.

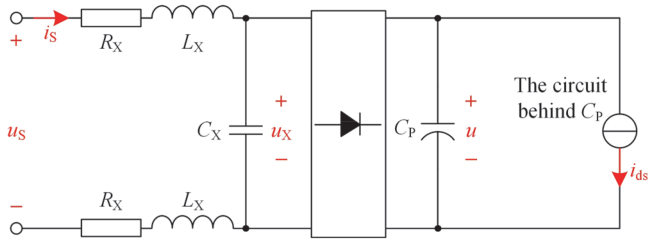

Fig. 4. Simplified excitation control circuit.

When u is a pulsating dc voltage and d_1 is maintained at d_{close}, ψ fluctuates with 2ω rad according to (14). By integrating the variation of ψ with the ω/π period, we can obtain

$$\begin{aligned}\Delta\psi_{\text{ave}} = & -2\sqrt{2}U_S d_{\text{close}}\left\{1-\exp\left[-\pi R/(\omega L)\right]\right\} \\ & \times\left(36\omega^2L^2+9R^2+4\omega LR\sin\theta+2R^2\cos\theta\right) \\ & \times\exp\left(-Rt/L\right)/\left[9\pi^2R\left(4\omega^2L^2+R^2\right)\right]. \quad (17)\end{aligned}$$

$\Delta\psi_{\text{ave}}$ tends to zero over time. Therefore, the fluctuating flux linkage is transformed into a stationary flux linkage ψ_{ave} by calculating the average value of ψ in the ω/π period. The state of the actuator can be estimated by the characteristics of ψ_{ave}. ψ_{ave} is calculated according to

$$\psi_{\text{ave}} = \psi_{\text{base}} + \sum\Delta\psi_{\text{ave}} \quad (18)$$

where ψ_{base} is the corresponding flux linkage when the coil current reaches its average value of the steady-state component I_{ave}. I_{ave} is obtained by R, L, U_S, and d_{close} according to (14).

At the beginning of the motion of the armature, the air gap does not change much, and L is L_{open} and does not change much. When i is stable, $\Delta\psi_{\text{ave}}$ decays to a small value, and ψ_{ave} remains. When the air gap decreases rapidly, L increases rapidly, the electromotive force makes i decline, and then ψ_{ave} increases. When the armature and stator are closed and the coil current is stable, ψ_{ave} remains constant.

According to the change in the ψ_{ave} waveform, a right triangle is established to describe the geometric feature of the flux linkage waveform. Based on the point at which the coil current reaches I_{ave}, the elapsed time Δt is the hook, and the difference between ψ_{ave} and ψ_{base} is the stock. The tangent value of the angle corresponding to the hook is

$$\tan Z = \left(\psi_{\text{ave}}-\psi_{\text{base}}\right)/\Delta t. \quad (19)$$

Taking the simulated flux linkage waveform of a 40 A contactor as an example, the right triangle is shown in Fig. 3. tan$Z$ will show a monotonicity reversion, which is the change from increasing to decreasing. A monotonicity reversion means that the contactor is in the closed position.

Because the voltage drops of semiconductor components and online estimation error of coil resistance affect the observation of ψ, the influence of ψ observation error on the monotonicity reversion of tan$Z$ needs to be further analyzed.

The error between the observed value and the true value of $\Delta\psi_{\text{ave}}$ in the nth calculation cycle is

$$\begin{aligned}e_{\Delta\psi(n)} &= \Delta\tilde{\psi}_{\text{ave}}-\Delta\psi_{\text{ave}} \\ &= \frac{\pi}{\omega}\left[i_{\text{ave}(n)}e_{\text{R}}+i_{\text{ave}(n)}R_{\text{on}}d_{\text{close}}+\left(1-d_{\text{close}}\right)u_{\text{F}}\right]\end{aligned} \quad (20)$$

where $\Delta\tilde{\psi}_{\text{ave}}$ is the observed $\Delta\psi_{\text{ave}}$ and u_{ave} and i_{ave} are the average values of u and i in the π/ω period, respectively.

We assume that the observation error of ψ_{base} is minimal. Then, the true value and observed value of tan$Z$ variation are

$$\begin{cases}\Delta_{\tan(n)} = \omega\left(\Delta\psi_{\text{ave}(n)}-\tan Z_{(n-1)}\right)/(\pi n) \\ \tilde{\Delta}_{\tan(n)} = \omega\left(\Delta\tilde{\psi}_{\text{ave}(n)}-\tan\tilde{Z}_{(n-1)}\right)/(\pi n)\end{cases} \quad (21)$$

where $\Delta_{\tan(n)}$ is the true value of tan$Z$ variation, $\tilde{\Delta}_{\tan(n)}$ is the observed value, and $\tan\tilde{Z}$ is the observed tan$Z$. Then,

$$\begin{aligned}\tilde{\Delta}_{\tan(n)} = & \Delta_{\tan(n)}+\omega e_{\Delta\psi(n)}/(\pi n) \\ & -\left(\omega^2\sum_{j=1}^{n}e_{\Delta\psi(j)}\right)/\left(\pi^2 n\left(n-1\right)\right).\end{aligned} \quad (22)$$

When i_{ave} is constant and n is large, $\Delta_{\tan(n)}\approx\tilde{\Delta}_{\tan(n)}$. When the electromotive force makes the coil current decline, the decrease in i_{ave} results in a decrease in $e_{\Delta\psi(n)}$, and $\Delta_{\tan(n)}\approx\tilde{\Delta}_{\tan(n)}$. Therefore, the geometric feature described in (19) has good compatibility with flux linkage observation error.

V. Self-Tuning Regulator for the LPO State

When the contactor is in the closed position, the coil current should be as large as possible to increase the electromagnetic force to resist external impact on the premise that the contactor's power consumption meets the demand. At the same time, the PI control parameters should minimize the coil current fluctuation to reduce high-frequency noise [23].

A. Coil Current Reference

The excitation control circuit can be simplified as shown in Fig. 4 in the LPO state. u_S and i_S are the voltage and current of the control power supply, respectively. R_X is the parasitic resistance of differential mode inductor L_X. u_X is the voltage of the differential mode capacitor C_X. u is the bus voltage. C_p is the rectifier filter capacitor. There is $u_X\approx u$ by ignoring the rectifier bridge voltage drop. i_{ds} is the drain-to-source current of

VT_1. i_{ds} is a rectangular wave whose period is the PWM period T_{PWM}, and i_{ds} can be described as

$$i_{ds} = I_{hold}\,\varepsilon\,(T_{PWM}d_1 - t) \tag{23}$$

where I_{hold} is the current reference and ε is the unit step function.

The charge consumed in the n-th PWM cycle is

$$\Delta\,Q_{(n)} = I_{hold}^2 R T_{PWM}/u_{(n)} \tag{24}$$

where $d_{1(n)} = I_{hold}R/u_{(n)}$.

C_P results in two kinds of relationships between u_S and u. One is $u \approx u_S$, and the other is $u > u_S$. The relationships between u_S and u affect the change in i_S.

If $u \approx u_S$, the charge consumed by i_{ds} comes from C_P, C_X, and the control power supply. By assuming that the difference between u and u_S in the nth PWM cycle is constant, i_S is

$$i_{S(n)}\,(t) = i_{S(n)}\big|_{t=0}\exp\left(-R_X t/L_X\right) + I_{hold}^2 R T_{PWM} \times[1-\exp\left(-R_X t/L_X\right)]/\left[2\left(C_P+C_X\right)u_{(n)}R_X\right]. \tag{25}$$

The average i_S in this PWM cycle is

$$\langle i_S\rangle_{(n)} \approx i_{S(n)}\big|_{t=0}\left[1 - R_X T_{PWM}/\left(2L_X\right)\right] + I_{hold}^2 R T_{PWM}^2/\left[4\left(C_P + C_X\right)u_{(n)}L_X\right]. \tag{26}$$

If $u > u_S$, the charge only comes from the C_P. i_S is

$$i_{S(n)}\,(t) = i_{S(n)}\big|_{t=0}\exp\left(-R_X t/L_X\right). \tag{27}$$

The average i_S in this PWM cycle is

$$\langle i_S\rangle_{(n)} \approx i_{S(n)}\big|_{t=0}. \tag{28}$$

Therefore, the active power consumption P and apparent power consumption S of the driver with a contactor are

$$\begin{cases} P = \frac{\omega}{2\pi}\left(\sum_{j=0}^{m}\langle u_S\rangle_{(j)}\langle i_S\rangle_{(j)}\Big|_{u\approx u_S} + \sum_{j=0}^{n-m}\langle u_S\rangle_{(j)}\langle i_S\rangle_{(j)}\Big|_{u>u_S}\right) \\ S = U_S\sqrt{\frac{\omega}{2\pi}}\left(\sum_{j=0}^{m}\langle i_S\rangle_{(j)}^2\Big|_{u\approx u_S} + \sum_{j=0}^{n-m}\langle i_S\rangle_{(j)}^2\Big|_{u>u_S}\right)^{\frac{1}{2}} \end{cases} \tag{29}$$

where $\langle u_S\rangle$ is the average u_S in the PWM period.

It can be seen from (26), (28), and (29) that the main factors affecting P and S are R, I_{hold}, and the relationship between u and u_S when the component of the excitation control circuit and the type of control power supply are fixed. P and S have at least a quadratic relationship with I_{hold} and a linear relationship with R. Therefore, a gray box of the power consumption of the driver with contactors can be established by dummy loads and using the polynomial function to fit the experimental data, as Fig. 5 shows.

As Fig. 5 shows, in Step 1, 25 points are measured by dummy loads. In Step 2, cubic polynomials of S or P with respect to the dummy load resistance r under different output currents i of the driver are built. In Step 3, a cubic polynomial of S or P with respect to i under the coil resistance R is built. In Step 4, by the binary search method, a suitable current reference I_{hold} is found to bring S or P close to the aim, which is represented as S_{aim} or P_{aim}, respectively.

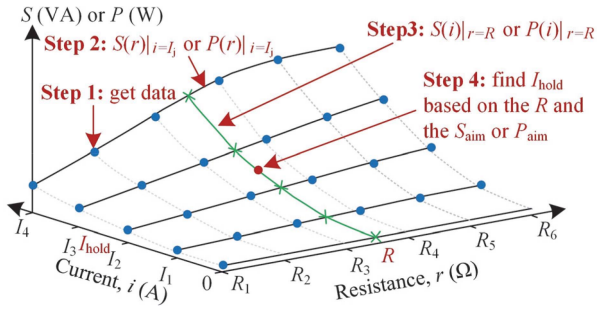

Fig. 5. Schematic diagram of the modeling process of the gray box.

B. PI Control Parameters

When the driver is in the LPO state, a PI controller is used to stabilize the coil current. PI control parameters can be configured based on the transfer function of the coil current control system.

When the coil current is stable, the current ripple is small, and the coil inductance is constant. We assume that the bus voltage is constant U. Therefore, the open-loop transfer function of the coil current control system is

$$G\,(s) = U\left(K_P s + K_I\right)/\left(s^2 L_{close} + sR\right) \tag{30}$$

where K_P is the proportional gain and K_I is the integral gain.

If $K_P \neq 0$ and $K_I = 0$, the root locus of the closed-loop coil current control system is in the negative real axis of the complex plane, and the system is always stable. Under the unit step input, the system has no overshoot with different K_P. The steady-state error of the system with the unit step input is

$$e_P\,(\infty) = R/\left(R + UK_P\right) \tag{31}$$

which K_P is set according to.

If $K_p \neq 0$ and $K_I \neq 0$, the closed-loop characteristic equation of the coil current control system is

$$D\,(s) = s^2\,L_{close} + s\left(UK_P + R\right) + UK_I. \tag{32}$$

This means that the closed-loop pole of the control system is always located to the left of the complex plane under different coil impedances, and the control system is always stable. If K_I meets

$$0 \le K_I \le \left(UK_P + R\right)^2/\left(4L_{close}U\right) \tag{33}$$

the pole of the closed-loop coil current control system is located on the negative real axis, the system is not underdamped, and the system has no overshoot under the unit step input, which is helpful to keep the PWM duty stable. K_I is larger, and the system becomes stable faster. Therefore, K_I should be as large as possible without overshooting the control system.

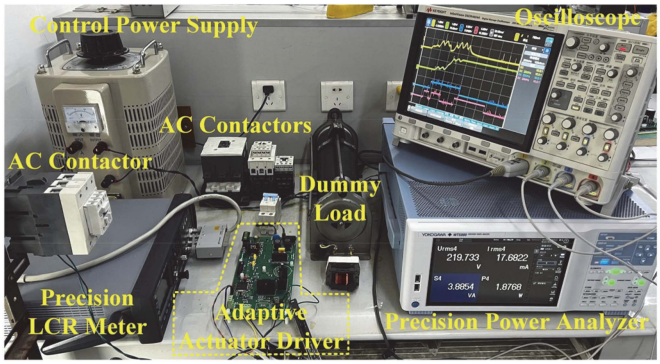

Fig. 6. Experimental setup.

TABLE I
COIL IMPEDANCES OF AC CONTACTORS

Rated contact current (A)	R (Ω)	L_{open} (H)	L_{close} (H)
18	499.2	1.686	17.998
40	158.5	0.726	12.461
95	120.2	0.611	11.219
170	76.6	0.439	6.102

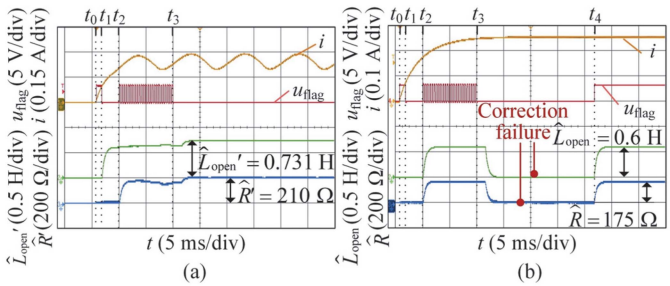

Fig. 7. Impedance estimation in (a) AC 220 V/50 Hz and (b) DC 220 V.

VI. EXPERIMENT

The prototype of the proposed adaptive actuator driver and four ac contactors are used in the experiment, as shown in Fig. 6. The driver has two interfaces. One interface is connected to the control power supply, and the other is connected to the coil of the contactor's actuator. The self-tuning regulators are embedded in STM32F103. The actuator of each contactor is equipped with a coil whose rated voltage is AC 220 V/50 Hz. The coil impedance is measured by a precision inductance–capacitance-resistance (LCR) meter, and the results are shown in Table I. A dummy load is used to establish the gray box. The working process and performance of the driver are assessed by an oscilloscope and a precision power analyzer.

A. Coil Impedance Estimation

The coil impedance estimation process is shown in Fig. 7. At t_0, excitation begins, and $d_1 = 0.2$ and $d_2 = 1$. To avoid the denominator of (2) being zero, the coil impedance is calculated by a fixed data point and a changing data point. The fixed data point is at t_1. The changing data point is from t_2 to t_3. The duration from t_0 to t_1 is 1 ms. The duration from t_1 to t_2 is 3 ms. After t_2, the coil resistance and coil inductance when the contactor is in the open position within 10 ms are estimated according to (2) and output by the digital-to-analog converter of STM32F103. At t_3, the estimation of coil impedance is corrected according to (5). In Fig. 7(b), the average coil impedance from t_2 to t_3 is output at t_4.

When the control power supply is dc, the estimated coil impedance is stable. The small diversity of the estimated results leads to the failure of estimation error correction. Therefore, the average coil resistance and coil inductance from t_2 to t_3 is regarded as the coil impedance result when the control power supply is dc.

During t_2–t_3, the periodic average filter is used to suppress the sampling noise of u and i. The more data points are put in the average filter, the better the filtering effect will be, but the larger the deviation between the sampling data and the real data of Δi will be. The data points used in the filter affect the coil impedance estimation accuracy. Fig. 8 shows the relative error of the estimated coil impedance with AC 220 V/50 Hz. The relative error comes from 10 estimation results. δ_R' and δ_L' are the relative errors of $\hat{R}'$ and $\hat{L}_{open}'$, respectively. δ_R and δ_L are the relative errors of $\hat{R}$ and $\hat{L}_{open}$, respectively. $\hat{R}$ and $\hat{L}_{open}$ are the average values of the estimated coil resistance and inductance from t_2 to t_3, respectively. δ_R and δ_R' decrease as the number of data points used in the filter increases. δ_L and δ_L' also decrease as the number of data points increases in a range. However, the larger the number of data points is, the greater the deviation between the sampling value and the true value of Δi. The greater deviation of Δi leads to δ_L and δ_L' increases. As shown in Fig. 8, with eight data points used in the filter, δ_R is generally lower than δ_R', δ_L' is generally lower than δ_L, and δ_R and δ_L'

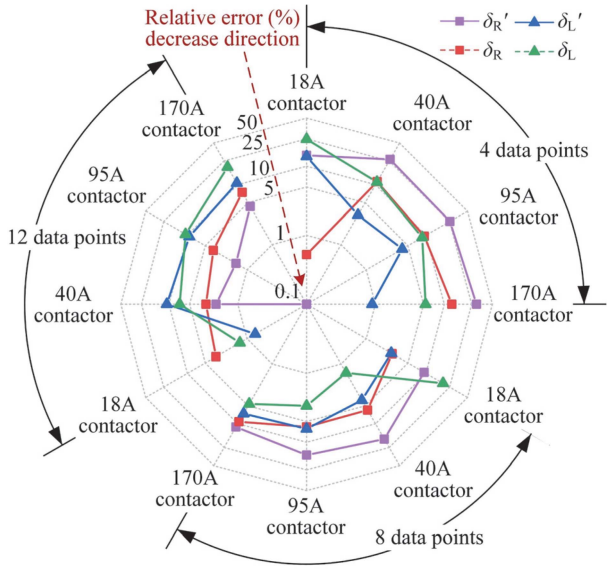

Fig. 8. Relative error of the estimated coil resistance and inductance with different numbers of data points used in the periodic average filter when the contactor is in the open position. The axis of relative error is logarithmic.

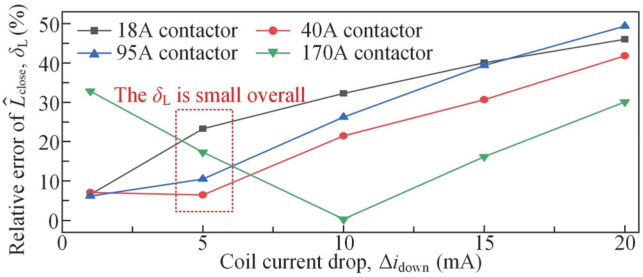

Fig. 9. Relative error of the estimated coil inductance with different coil current drops used in (7) when the contactor is in the closed position.

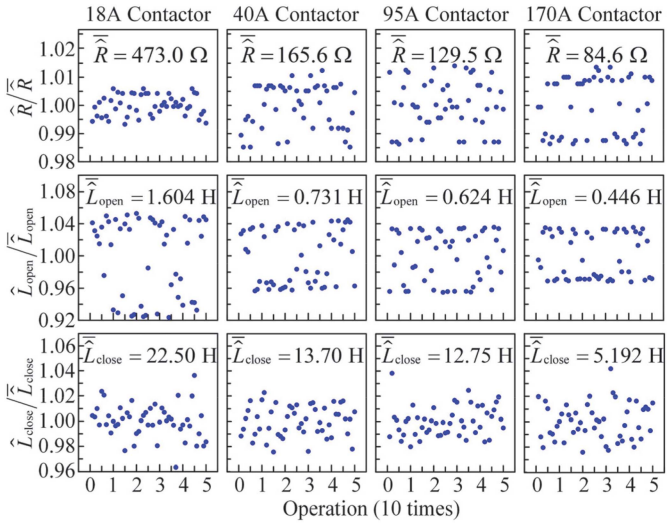

Fig. 10. Fluctuation of the coil impedance estimation.

are below 10%. Therefore, $\hat{R}$ and $\hat{L}'_{open}$ are taken as the estimation results when the control power supply is ac.

The relative error of coil inductance estimation based on (7) is analyzed, as shown in Fig. 9. In the experiment, the armature and stator of each contactor are closed reliably, and I_{hold} is 10 mA to ensure that the cores work in the linear region as much as possible.

In Fig. 9, the relative error δ_L comes from 10 estimation results. The increase in Δi_{down} is beneficial to suppress the effect of sampling noise but also leads to an increase in δ_L. On the premise of sufficient estimation accuracy, Δi_{down} should be as large as possible to ensure the stability of the estimation results. When Δi_{down} is 5 mA, the estimation error is small, and the estimation results are stable.

The stability of the coil impedance estimation is verified by 50 operations at AC 220 V/50 Hz, as shown in Fig. 10. These experimental results are represented in a unitized way with the average of all results. The variation coefficient of these results is less than 5%, and the maximum fluctuation is below 8% of the average. The coil impedance estimation results fluctuate little, and the coil impedance estimation scheme is stable.

TABLE II
VERIFICATION OF (16) BY DIFFERENT AC CONTACTORS AND (34)

Rated contact current (A)	$U_{close(min)}$ (V)	$U_{drive(min)}$ (V)	$U_{drive(min)}'$ (V)	δ_U (%)
18	140.6	106.8	100.3	6.1
40	161.2	102.0	111.2	9.0
95	152.0	89.5	87.6	2.1
170	145.5	78.4	75.8	3.3

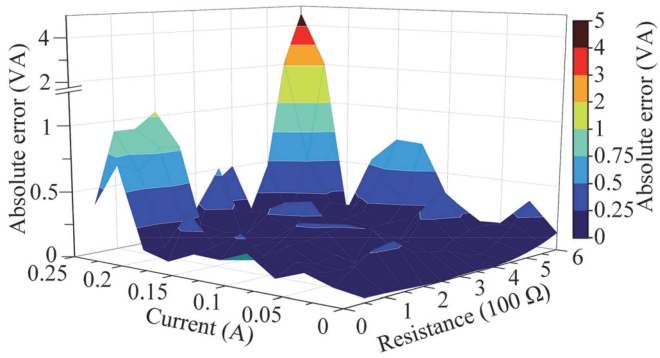

Fig. 11. Precision of the gray box of power consumption.

B. Mathematical Equations

The mathematical equations include (16), the gray box of power consumption, (31), and (33). Equations (31) and (33) can be verified by the working performance of the driver.

To verify (16), d_{close} is set to 1. Then, (16) can be counterproof based on the minimum control supply voltage when the contactor is equipped with the driver. The minimum control power supply voltage is

$$U_{drive(min)} = 9\pi R U_{close(min)} \sqrt{4\omega^2 L_{open}^2 + R^2} \Big/ \left[2\sqrt{2}\sqrt{\left(324\omega^2 L_{open}^2 + 83R^2\right)\left(\omega^2 L_{open}^2 + R^2\right)}\right] \quad (34)$$

where $U_{close(min)}$ is the minimum control power supply when the contactor is under ac excitation and is acquired by experiments. We note that the experimental $U_{drive(min)}$ is $U'_{drive(min)}$. Then, according to the experimental results shown in Table II, $U_{drive(min)}$ is similar to $U'_{drive(min)}$, the average of the relative error δ_U is approximately 5.1%, and the maximum value of δ_U is 9%, which indicates the validity of (16).

The verification experiment of the gray box is carried out at AC 220 V/50 Hz. The experimental setup is that the resistance of the dummy load is from 50 to 600 Ω in 50 Ω increments, and the driver output current is from 0 to 0.25 A in 0.025 A increments. The gray box is established by 25 experimental data points. The absolute error of the gray box is shown in Fig. 11. The maximum absolute error is 4.61 VA, the average is 0.26 VA, the maximum relative error is 9.23%, and the average relative error is 2.14%. The gray box has good accuracy.

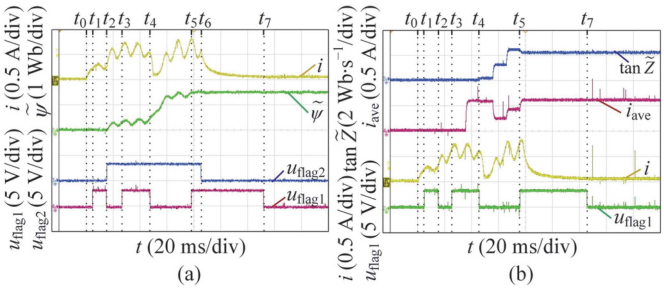

Fig. 12. Working process of the adaptive actuator driver with a 40 A contactor. Some parameters and flags are shown in (a) and (b). u_{flag1} is the flag of the control stages. u_{flag2} is the flag of the I_{hold} calculation state.

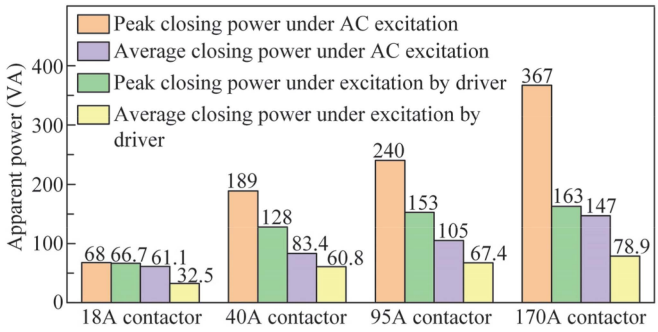

Fig. 13. Comparison of power during the motion of the armature.

C. Working Process

The 40 A contactor is taken as an example to show the working process of the proposed adaptive actuator driver, as shown in Fig. 12. At t_0, the excitation begins with a small PWM duty, and the coil current increases slowly. From t_1 to t_2, the driver acquires data to estimate the coil impedance. After t_2, d_{close} is set, and the driver enters the HPO state. At the same time, the flux linkage of the actuator is observed, and the calculation of I_{hold} starts. At t_3, the coil current reaches the estimated average value of the steady-state component. At this moment, the flux linkage is regarded as ψ_{base}. Then, the average coil current i_{ave} and $\tan \tilde{Z}$ are calculated within a periodic 10 ms cycle. i_{ave} is used as an auxiliary criterion for the position identification of the actuator to avoid misidentification caused by the small fluctuations of $\tan \tilde{Z}$ at the beginning of the motion of the armature. At t_4, i_{ave} decreases, and the driver considers that the contactor is about to be in the closed position. At t_5, the monotonicity of $\tan \tilde{Z}$ reverses, and the driver judges that the armature and stator have been closed stably. At t_6, the calculation of I_{hold} is complete. When I_{hold} is set and the contactor is judged to be at the closed position, the driver enters the LPO state, and the coil current starts to decline. At t_7, the PI control parameters are set according to the coil impedance, and then the coil current is maintained at I_{hold}.

Orthogonal experiments are carried out with the combination of the ac or dc control power supply, four specifications of contactors, and control supply voltage ($85\%U_{\text{e}}$, U_{e}, or $110\%U_{\text{e}}$). The experimental results show that the driver can adapt to the changes in the contactor specifications and that the contactors with the driver work reliably.

D. Working Performance

The adaptive actuator driver can reduce the power consumption of traditional contactors. The power consumption during the motion of the armature is reduced by suppressing the harmonic current of the control power supply with the electromagnetic compatible filter and the constant PWM duty. The power consumption when the contactor is in the closed position is reduced by lowering the coil current amplitude.

TABLE III
STABILITY ANALYSIS OF THE COIL CURRENT IN THE LPO STATE

Rated contact current (A)	Average coil current, $\bar{I}_{\text{hold}}$ (mA)	Standard deviation (mA)	Variable coefficient (%)
18	44.67	0.276	0.62
40	77.45	0.552	0.71
95	91.22	0.627	0.69
170	118.05	0.679	0.58

The power consumption during the motion of the armature can be described by the peak closing power and average closing power. The peak closing power is obtained by multiplying the peak control supply current and its corresponding control supply voltage from the beginning of excitation to the closure of contacts and both dividing $\sqrt{2}$ when the control power supply is ac or do nothing when the control power supply is dc. The average closing power is obtained by multiplying the RMS of the control supply voltage and the RMS of the control supply current from the beginning of excitation to the closure of contacts. It can be seen from Fig. 13 that the driver reduces the power consumption to 65% on average and 44% on minimum.

Further experiments on the stability of the LPO state are carried out. Table III shows the experimental results. The experimental conditions are as follows: the control power supply is AC 220 V/50 Hz, $e_{\text{P}}(\infty)$ is 0.1, and S_{aim} is 5 VA according to the power consumption standard (GB21518). The data in Table III come from 10 operations. In the LPO state, the standard deviation of the coil current is below 0.7 mA and the maximum variation coefficient is approximately 0.7%, which means that the self-tuning of the coil current reference is stable.

Due to the inertia of the contactor control system, which adopts PI control in the LPO state, the coil current will first be lower than the current reference and then gradually rise to the current reference during the transition from the HPO state to the LPO state. The experimental results of different contactors with different ac control supply voltages are shown in Table IV. Δi_{down} is the maximum amplitude when the coil current is below the reference. Δi_{rip} is the current ripple when the coil current is stable. By analyzing the results in Table IV with Table III, we can see that $\Delta i_{\text{down}}/\bar{I}_{\text{hold}}$ is below 6%, Δi_{rip} is 3–4 mA, and $\Delta i_{\text{rip}}/\bar{I}_{\text{hold}}$ is below 7%. The results mean that the self-tuning regulator of PI control parameters is effective.

TABLE IV
ANALYSIS OF COIL CURRENT CHANGE DURING THE TRANSITION

Rated contact current (A)	U_S (V)	Δi_{down} (mA)	$(\Delta i_{down}/\bar{I}_{hold})$ (%)	Δi_{rip} (mA)	$\Delta i_{rip}/\bar{I}_{hold}$ (%)
18	187	1.88	4.20	2.95	6.60
	220	1.79	4.00	2.84	6.36
	242	1.43	3.19	3.01	6.74
40	187	3.25	4.20	3.34	4.31
	220	4.00	5.16	3.18	4.11
	242	4.20	5.42	3.00	3.87
95	187	4.30	4.71	3.18	3.49
	220	4.75	5.21	3.01	3.30
	242	4.75	5.21	2.92	3.20
170	187	6.50	5.51	3.68	3.12
	220	6.75	5.72	3.60	3.05
	242	7.00	5.93	4.00	3.39

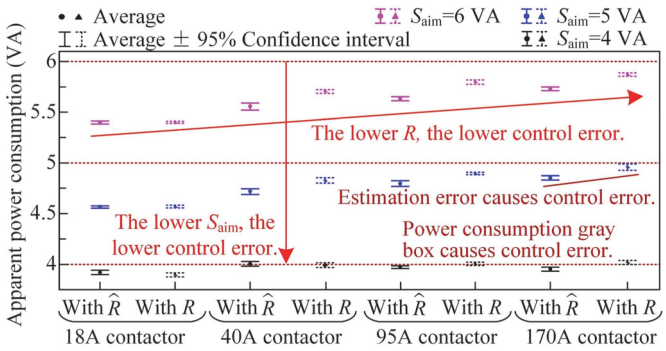

Fig. 14. Power consumption in the LPO state.

The experimental results of the power consumption in the LPO state are shown in Fig. 14. The data in Fig. 14 come from 10 operations. The estimation error of the coil resistance affects the control accuracy of power consumption, and its influence decreases gradually with decreasing coil resistance. However, the actual power consumption cannot always be the same as the aim S_{aim}, even if the true coil resistance is used for the self-tuning of the coil current reference I_{hold} in the LPO state. The reason is that the estimation error of I_{hold} comes not only from the coil resistance estimation but also from the gray box. When R or S_{aim} is lower, the change rate of the power consumption with the coil current is smaller, the control error caused by the I_{hold} estimation error is smaller, and the actual power consumption is closer to the aim.

VII. CONCLUSION

In this article, an adaptive actuator driver is established based on the coil impedance estimation, mathematical equations between the coil impedance and control parameters, and a geometric feature of flux linkage waveform. The coil impedance estimation was fast and accurate. The mathematical equations minimized the dependence of excitation control parameters self-tuning on the contactor structural parameters. The self-transition of the driver's working state was achieved without a threshold using the geometric feature, which is compatible with the flux linkage observation error. Therefore, the proposed adaptive actuator driver has a one-to-many relationship with the contactors, the advantages of the fast self-tuning of excitation control parameters, and a plug-and-play function on different contactors. This driver is convenient and suitable for traditional ac contactors that are in service to realize energy-saving operation. In the future, this driver can be developed as a chip or an accessory for contactors, which is helpful to reduce the resource input of the development and productization of the contactors controlled by electronic modules and accelerate the intelligentization of contactors.

REFERENCES

[1] L. Yao, X. Xiao, Y. Wang, and W. Xu, "Adaptive contactor—A new scheme to improve induction motor immunity to voltage sags," *IEEE Trans. Power Del.*, vol. 36, no. 6, pp. 3360–3370, Dec. 2021, doi: 10.1109/TPWRD.2020.3038947.

[2] K. Subramaniam and M. S. Illindala, "Intelligent three tie contactor switch unit-based fault detection and isolation in DC microgrids," *IEEE Trans. Ind. Appl.*, vol. 56, no. 1, pp. 95–105, Jan./Feb. 2020, doi: 10.1109/TIA.2019.2948923.

[3] I. A. Pires, A. A. P. Machado, and B. de Jesus Cardoso Filho, "Mitigation of electric arc furnace transformer inrush current using soft-starter-based controlled energization," *IEEE Trans. Ind. Appl.*, vol. 54, no. 4, pp. 3909–3918, Jul./Aug. 2018, doi: 10.1109/TIA.2018.2825240.

[4] N. Gabdullin and J.-S. Ro, "Energy-efficient eco-friendly zero-holding-energy magnetic contactor for industrial and vehicular applications," *IEEE Trans. Veh. Technol.*, vol. 69, no. 5, pp. 5000–5011, May 2020, doi: 10.1109/TVT.2020.2981888.

[5] S. Fang, Y. Chen, and Y. Yang, "Optimization design and energy-saving control strategy of high power dc contactor," *Int. J. Elect. Power Energy Syst.*, vol. 117, May 2020, Art. no. 105633, doi: 10.1016/j.ijepes.2019.105633.

[6] H. Lin, X. Wang, S. Fang, P. Jin, and S. L. Ho, "Design, optimization, and intelligent control of permanent-magnet contactor," *IEEE Trans. Ind. Electron.*, vol. 60, no. 11, pp. 5148–5159, Nov. 2013, doi: 10.1109/TIE.2012.2227907.

[7] X. Xiao, H. He, and Y. Wang, "Analytical model of AC contactors for studying response mechanism to multi-dimensional voltage sag characteristics and its novel applications," *IET Gener., Transmiss. Distrib.*, vol. 13, no. 17, pp. 3910–3920, Sep. 2019, doi: 10.1049/iet-gtd.2018.7077.

[8] L. Tang and Z. Xu, "The control technology of self-correction for intelligent AC contactors," *Zhongguo Dianji Gongcheng Xuebao/Proc. Chin. Soc. Elect. Eng.*, vol. 35, no. 6, pp. 1516–1523, Mar. 2015.

[9] P. M. D. S. D. de Moraes and A. J. Perin, "An electronic control unit for reducing contact bounce in electromagnetic contactors," *IEEE Trans. Ind. Electron.*, vol. 55, no. 2, pp. 861–870, Feb. 2008, doi: 10.1109/TIE.2007.909073.

[10] S. Fang, Y. Chen, and H. Lin, "A self-adaptive control for phase-controlled electromagnetic contactor using weighted moving average filter," *IEEE Trans. Ind. Electron.*, vol. 68, no. 9, pp. 8963–8972, Sep. 2021, doi: 10.1109/TIE.2020.3016268.

[11] C. Zhang and Z. Xu, "A cascade control strategy for intelligent AC contactors based on flux linkage feedback," *Zhongguo Dianji Gongcheng Xuebao/Proc. Chin. Soc. Elect. Eng.*, vol. 40, no. 4, pp. 1329–1338, Feb. 2020.

[12] L. Tang, W. Chen, and Z. Xu, "The self-correcting control strategy of a single flux linkage closed loop for a contactor," *IEEE Trans. Ind. Electron.*, vol. 69, no. 11, pp. 11521–11530, Nov. 2022, doi: 10.1109/TIE.2021.3125560.

[13] E. Ramirez-Laboreo, C. Sagues, and S. Llorente, "A new run-to-run approach for reducing contact bounce in electromagnetic switches," *IEEE Trans. Ind. Electron.*, vol. 64, no. 1, pp. 535–543, Jan. 2017, doi: 10.1109/TIE.2016.2605622.

[14] Z. Wu, G. Wu, C. Chen, Y. Fang, L. Pan, and H. Huang, "A novel breaking strategy for electrical endurance extension of electromagnetic alternating current contactors," *IEEE Trans. Compon., Packag. Manuf. Technol.*, vol. 6, no. 5, pp. 749–756, May 2016, doi: 10.1109/TCPMT.2016.2542101.

[15] L. Tang, Z. Han, and Z. Xu, "A sequential adaptive control strategy for the contact colliding speed of contactors based on fuzzy control," *IEEE Trans. Ind. Electron.*, vol. 68, no. 7, pp. 6064–6074, Jul. 2021, doi: 10.1109/TIE.2020.2994872.

[16] A. G. Espinosa, J. R. R. Ruiz, J. Cusidó, J. A. Ortega, and L. Romeral, "Closed-loop controller for eliminating the contact bounce in DC core contactors," *IEEE Trans. Compon., Packag. Technol.*, vol. 33, no. 3, pp. 535–543, Sep. 2010, doi: 10.1109/TCAPT.2010.2041456.

[17] T. Longfei, H. Zhiping, and X. Zhihong, "Neural network-based co-simulation technology for intelligent contactors," *IEEE Trans. Magn.*, vol. 56, no. 2, Feb. 2020, Art. no. 8000108, doi: 10.1109/TMAG.2019.2948318.

[18] S. Sun, Q. Wang, T. Du, J. Wang, S. Li, and J. Zong, "Quantitative evaluation of electrical life of AC contactor based on initial characteristic parameters," *IEEE Trans. Instrum. Meas.*, vol. 70, 2021, Art. no. 3503510, doi: 10.1109/TIM.2020.3031160.

[19] L. Liu, W. Yang, Y. Chai, J. Guo, and G. Zhai, "A new theoretical model to study the closing bounce characteristics of the electromagnetic relay under capacitive loads," *IEEE Trans. Compon., Packag. Manuf. Technol.*, vol. 10, no. 8, pp. 1358–1366, Aug. 2020, doi: 10.1109/TCPMT.2020.3011515.

[20] C. Zhang and Z. Xu, "A digital controller for series of AC contactors," in *Proc. IEEE 5th Int. Conf. Electric Power Equip. Switching Technol.*, 2019, pp. 702–705, doi: 10.1109/ICEPE-ST.2019.8928750.

[21] C. Zhang and Z. Xu, "Sensorless online opening time estimation of contactors," *Zhongguo Dianji Gongcheng Xuebao/Proc. Chin. Soc. Elect. Eng.*, vol. 42, no. 10, pp. 3805–3814, May 2022.

[22] R. W. Erickson, "Circuit averaging, averaged switch modeling, and simulation," in *Fundamentals of Power Electronics*, D. Maksimović, Ed. Berlin, Germany: Springer, 2020, pp. 548–558.

[23] L. Tang, J. Zhuang, H. Sun, and Z. Xu, "Suppression strategies of electromagnetic switch high-frequency holding noise," *Diangong Jishu Xuebao/Trans. Chin. Electrotechn. Soc.*, vol. 37, no. 10, pp. 2631–2643, May 2022.

Changkun Zhang was born in Yichun, Heilongjiang, China, in 1994. He received the Ph.D. degree in electric machines and electric apparatus from the Fuzhou University, Fuzhou, Fujian, China, in 2022.

He is currently working with the School of Marine Engineering, Jimei University, Xiamen, China. His research interests include electrical apparatuses and intelligent technologies.

Zhihong Xu (Member, IEEE) was born in Linfen, Shanxi, China in 1963. She received the M.S. degree in electronic engineering and Ph.D. degree in electric machines and electric apparatus from the Fuzhou University, Fuzhou, Fujian, China, in 1998 and 2006, respectively.

Since August 1983, she has been working with Fuzhou University, Fuzhou, Fujian, China. She was elected professor in 2006. She has been the Dean of the College of Electrical Engineering and Automation since June 2016. Her research interests include electrical apparatuses and intelligent technologies.